REDV-modified decellularized microvascular grafts for arterial and venous reconstruction

Short running title: REDV-conjugated Microvascular Grafts

Hiroki Yamanaka, MD, PhD[1,2]; Atsushi Mahara, PhD[1]; Naoki Morimoto, MD, PhD[2]; Tetsuji Yamaoka, PhD[1]

[1]Department of Biomedical Engineering, National Cerebral and Cardiovascular Center Research Institute, 6-1 Kishibe-Shimmachi, Suita, Osaka 564-8565, Japan.

[2]Department of Plastic and Reconstructive Surgery, Graduate School of Medicine and Faculty of Medicine, Kyoto University, 54 Shogoin Kawahara-cho, Sakyo-ku, Kyoto 606-8507, Japan

Corresponding author: Tetsuji Yamaoka, PhD

Department of Biomedical Engineering, National Cerebral and Cardiovascular Center Research Institute, 6-1 Kishibe-Shimmachi, Suita, Osaka 564-8565, Japan.

E-mail: yamtet@ncvc.go.jp

Tel: +81-6-6170-1070, ext. 31009

Acknowledgments

The authors thank Dr. Koko Asakura (Department of Data Science, National Cerebral and Cardiovascular Center, Japan) for providing helpful comments on the statistical analysis. This research was supported by the Japan Agency for Medical Research and Development (AMED) S-Innovation Program for the development of biofunctional materials for the realization of innovative medicine.

Data availability

The data that support the findings of this study are available from the corresponding author, Tetsuji Yamaoka, upon reasonable request.

Declarations of interest: none

Ethics approval

All animal experiments were conducted in accordance with the guidelines for animal experiments established by the Ministry of Health, Labor and Welfare of Japan and by the National Cerebral and Cardiovascular Center Research Institute, Japan. The

protocol was approved by the Committee on the Ethics of Animal Experiments of the National Cerebral and Cardiovascular Center Research Institute (Permit Number 18035).

Abstract

Recently, a decellularized microvascular graft (inner diameter: 0.6 mm) modified with the integrin α4β1 ligand, REDV, was developed to provide an alternative to autologous-vein grafting in reconstructive microsurgery, showing good early-stage patency under arterial flow in rats. This consecutive study evaluated its potential utility not only as an arterial substitute, but also as a venous substitute, using a rat-tail replantation model. Graft remodeling depending on hemodynamic status was also investigated. ACI rat tail arteries were decellularized via ultra-high-hydrostatic pressure treatment and modified with REDV to induce antithrombogenic interfaces and promote endothelialization after implantation. Grafts were implanted into the tail artery and vein to re-establish blood circulation in amputated Lewis rat tails (n =12). The primary endpoint was the survival of replants. Secondary endpoints were graft patency, remodeling, and regeneration for 6 months. In all but three cases with technical errors or postoperative self-mutilation, tails survived without any evidence of ischemia or congestion. Six-month Kaplan-Meier patency was 100% for tail-artery implanted grafts and 62% for tail-vein implanted grafts. At 6 months, the neo-tunica media (thickness: 95.0 μm in tail-artery implanted grafts, 9.3 μm in tail-vein implanted grafts) was regenerated inside the neo-intima. In conclusion,

the microvascular grafts functioned well both as arterial and venous paths of replanted-rat tails, with different remodeling under arterial and venous conditions.

Keywords: tissue engineering; decellularized; microvascular graft; replantation; integrin α4β1

1. Introduction

In the field of microvascular surgery, including free-tissue transfer and replantation surgery, autologous veins are the first-choice conduit for the elongation or replacement of tissue vascular pedicles. They are used for arteries and/or veins in 2–30% of microsurgeries with satisfactory results;[1-4] however, this strategy has some disadvantages including limited sources, time required to harvest, and donor-site morbidities.[5,6] In addition, some patients have no available vein as a result of prior removal for cosmetic or surgical procedures, or because of severe peripheral vascular disease.[7] The development of vascular prostheses with inner diameters (ID) < 3 mm (microvascular prostheses: m-VPs) may provides an alternative to autologous vein grafts in reconstructive microsurgery. Ideally, m-VPs should have reliable patency, even in very-small-diameter vessels; moreover, they should be available in different sizes and lengths as both arterial and venous substitutes. Currently available synthetic materials (e.g., expanded polytetrafluoroethylene) are usable only for large-diameter vessels but not for microsurgical requirements because of their thrombogenicity. In particular, it is a challenge to achieve high patency under venous conditions, in which the flow rate is too slow to flush blood clots in the graft lumen.[8] It is assumed that tissue-engineering

strategies are necessary to develop clinically useful m-VPs.

Since the first constructed tissue-engineered vascular graft (TEVG) was reported by Weinberg and Bell in 1986,[9] researchers have made great efforts to create cell-based, live TEVGs that can function immediately post-implantation.[10,11] Several cell-based TEVGs have been successfully used in clinical trials; however, their manufacture involves patient cell culture, which is time consuming and expensive.[11-13] Consequently, recent trends in vascular tissue engineering have been focused on the development of cell-free, scaffold-based grafts that are capable of hospital storage and readily available for on-demand surgeries.[13] To date, multiple materials, including biodegradable synthetic polymers, natural polymers, and decellularized tissues, have been investigated as scaffolds. Among these, decellularized blood vessels are potentially advantageous because of their similarity to native tissues in terms of their complex vascular wall structure, biomechanical properties, and multiple biological functions.[13-15] In addition, they can be readily handled, manipulated, and sutured, thereby making them immensely suitable for implantation. On the other hand, decellularized tissues have thrombogenic properties, since the primary component of the extracellular matrix, collagen, can interact with the von Willebrand factor and blood coagulation proteins, promoting platelet adhesion.[10] Moreover, readily available decellularized tissue-based grafts, such as

Procol®, Solcograft®, Artegraft®, and Synergraft®, are not clinically satisfactory.[14] Recent studies suggest that early confluent endothelialization and inhibition of thrombosis are the most important steps that enhance the patency of cell-free grafts.[7,10,11,16-21] However, the details of host responses to these biological approaches to improve the blood-contact interface of decellularized blood vessels remain unclear.[22-24]

We previously reported a novel luminal modification method for producing decellularized tissues, using the synthetic peptide (Pro-Hyp-Gly)$_7$-Gly-Gly-Gly-Arg-Glu-Asp-Val (CMP-REDV) comprising collagen mimetic peptides (CMPs; (POG)$_7$), a linker (GGG), and an integrin-α4β1 ligand (REDV).[7,20,25] The peptide REDV has high affinity for endothelial and endothelial progenitor cells, and shows anti-platelet adhesion properties.[26] When CMP-REDV was immobilized on decellularized ostrich carotid arteries (ID 2–4 mm, length >30 cm), *in vivo* experiments using a mini-pig femoral-femoral bypass model showed that it actually contributed to rapid re-endothelialization, suppressing early thrombus formation.[25] Theoretically, this luminal-modification method can be applied any size of decellularized blood vessels; in other words, it is possible to manufacture a novel m-VP series covering a range of sizes. Focusing on the submillimeter-diameter range, we prepared CMP-REDV-conjugated microvascular grafts from decellularized rat-tail arteries (ID: 0.6 mm). On the basis of

previous experiments showing their high antithrombogenicity under arterial flow,[7] this study aimed to evaluate their applicability for venous reconstruction and to assess and compare the remodeling of artery-implanted and venin-implanted grafts. Allografts were implanted to reconstruct both arterial supply and venous drainage of fully amputated-rat tails. The primary endpoint was the survival rate of replanted tails. Tail viability was evaluated by analyzing skin-blood flow with laser-speckle contrast imaging. Secondary endpoints were graft patency and graft remodeling and regeneration for up to 6 months.

2. Materials and Methods

All animal experiments were conducted in accordance with the guidelines for animal experiments established by the Ministry of Health, Labor and Welfare of Japan and by the National Cerebral and Cardiovascular Center Research Institute, Japan. The protocol was approved by the Committee on the Ethics of Animal Experiments of the National Cerebral and Cardiovascular Center Research Institute (Permit Number: 18035).

2.1 Graft preparation

Decellularized rat-tail arteries were prepared by using ultrahigh-hydrostatic pressure (UHP) treatment as previously reported.[7] Tail arteries, 5–8 cm in length, were harvested from ACI rats (190–210 g; Japan SLC, Inc., Hamamatsu, Japan). Blood remaining in the lumen of the tail arteries was flushed with heparinized saline solution. Samples were pressurized at 1000 MPa for 10 min using a Dr. Chef high-pressure food processor (Kobe Steel, Ltd., Kobe, Japan). Both increasing the pressure to 1000 MPa and decreasing it to atmospheric pressure required 15 min. Following pressurization, the sample was incubated in saline containing 40 U/mL DNase I (Roche Applied Science, Indianapolis, IN, USA), 20 mM $MgCl_2$, 100 U/mL penicillin, and 100 μg/mL streptomycin (Pen/Strep; Gibco, Life Technologies, Carlsbad, CA, USA) for 24 h at 37 °C. The sample was then washed with saline containing 500 mg/L ethylenediaminetetraacetic acid (EDTA) and the same antibiotics to remove remaining DNase I and Mg^{2+}, and stored in the same solution at 4 °C. Decellularized arteries were divided into three groups: ID was measured for one, another was histologically evaluated, and the third was modified with CMP-REDV (Sigma-Aldrich Japan Corp., Tokyo, Japan) for *in vivo* experiments.

Luminal modification was performed within 5 d after harvesting. Several reports have described that CMPs have triple-helical structures and reversible melting behavior similar to that of natural collagen; moreover, monomeric CMPs interact with denatured

collagen via strand invasion.[27,28] The peptide CMP-REDV was dissolved in saline and stored in the stable, trimeric form at 4 °C until experimental usage. First, a 10 μM peptide solution was heated to 60 °C for 5 min to thermally dissociate the peptides to monomers. The heated peptide solution was then rapidly cooled to ambient temperature. Thereafter, decellularized vessels were filled with the quenched peptide solution, clamped at both ends, and immersed in the solution at 4 °C for > 24 h. When the heated peptide solution was cooled immediately before peptide modification, the active monomeric peptides were predominant in the solution until exposed to the decellularized scaffolds (dead time < 2 min).[29] The CMP-REDV-conjugated microvascular grafts were implanted within 3 days after peptide modification.

To verify the interaction between monomeric peptides and pressurized collagen, CMP-REDVs were labeled with Alexa Fluor 633 NHS esters (Thermo Fisher Scientific, Inc., Waltham, MA, USA).[7] Native arteries and 1000-MPa-pressurized arteries were generated. Cross sections (8 μm) of these frozen samples were produced and labeled with either non-heated trimeric peptides or heated-and-cooled monomeric peptides at 4 °C overnight (n = 6). After washing with PBS at ambient temperature (approximately 20 °C) for 1 h, we evaluated peptide binding via confocal laser-scanning microscopy (CLSM). Fluorescence intensity was analyzed as mean gray values, using ImageJ

software (version: 2.0.0-rc-69/1.52i). Tail arteries pressurized at 0, 50, 100, 200, 500, and 1000 MPa were also generated (n = 3 for each), labeled with monomeric peptides, and evaluated via CLSM.

2.2 *In vivo* experiments

In vivo experiments were conducted in high-responder, completely MHC-mismatched, ACI-to-Lewis rat models.[30] Male Lewis rats (8 weeks, 250–270 g; Japan SLC, Inc.) were used as recipients. Before graft implantations, two control groups were formed: a rat-tail devascularization model and a rat-tail venous congestion model (n = 3 for each). For the former, the Lewis rat tail was completely amputated once and then sutured back onto the original location without vessel reconstruction. For the latter, the Lewis rat tail was amputated except for the tail artery, then sutured back onto the original location without venous reconstruction. Blood flow in the re-sutured tails was analyzed via laser-speckle contrast imaging (moorFLPI-1; Zero C Seven, Inc., Tokyo, Japan). After 3 days of follow-up, the rats were euthanized.

In the study group, 12 rats underwent tail replantation using CMP-REDV-conjugated microvascular grafts (no sample size calculation and animal blinding were performed). Upon anesthesia induction and systematic administration of 200 IU/kg heparin,

skin-blood flow of the native tail was evaluated using moorFLPI-1. A silicon tube was applied on the base of the tail as a tourniquet. The tail was completely amputated at a position 1.5 cm distal to its base. Skin-blood flow of the amputated tail was also evaluated with moorFLPI-1. Skin incisions, 1 cm long, were made at the right lateral side of both the base of the tail and the stump of the amputated tail. The tail artery and one of the two superficial veins were exposed and isolated. The distal tail was reattached with four mattress sutures, using 5-0 polypropylene (Prolene; Ethicon, Inc., Johnson & Johnson K.K., Tokyo, Japan) through the tendons and periosteum. On resecting the native vessel from each transection by a few millimeters, the interposition graft (8 mm long) was anastomosed to reconstruct the tail artery in an end-to-end manner with 6–8 interrupted 11-0 nylon sutures (Microsurgery suture DL-2.5; Kono Seisakusho, Co., Ltd., Tokyo, Japan). The 5-mm interposition graft was similarly anastomosed to the right superficial vein. Following anastomoses, the tourniquet was deflated (ischemia time: 108 ± 18 min) and immediate patency was assessed using the empty-and-refill (milking) test.[31] The skin was closed using interrupted 5-0 polypropylene sutures. In all but the first case, a local advancement flap was used to reduce skin tension in the primary skin closure.

Three rats were excluded from postoperative analyses because of intraoperative

technical errors or postoperative self-mutilation. After 3 weeks, 3 months, and 6 months, skin-blood flow in the replanted tails was evaluated via moorFLPI-1; the scanning model had a high-resolution setting and an exposure time of 4 ms, with 100 frames processed on average into a single image to obtain the mean flux; the whole tail area was selected as a region of interest and median flux value was analyzed using the Image Review Program of Moor-FLPI-V3.0 software. Also, patency of the tail-artery implanted grafts (arterial grafts) was determined at 3 weeks, 3 months, and 6 months, using pulsed-wave and color Doppler ultrasound (Prosound II, SSD-6500 SV; Hitachi Aloka Medical, Ltd., Tokyo, Japan). Patency of the tail-vein implanted grafts (venous grafts) was directly examined via the milking test at 3 weeks, 3 months, and 6 months, since venous flow was too slow to be detected using ultrasound. The direct patency test was not performed until 3 weeks, since the test itself may be invasive enough to affect the patency rate, particularly at early stages after implantation. At predetermined time points (n = 3 each for 3 weeks, 3 months, and 6 months), full-length implanted grafts, including both the proximal and distal anastomoses, were extracted and the rats were euthanized.

2.4 Histology

Samples were longitudinally sectioned, fixed with 10% formalin (Wako Pure Chemical Industries, Ltd., Osaka, Japan) for 2 h, and stored in PBS at 4 °C. Histological staining (hematoxylin and eosin (HE) staining, Elastica van Gieson (EVG) staining, α-smooth muscle actin (αSMA) staining, and CD31 immunostaining) was carried out at the Applied Medical Research Laboratory (Osaka, Japan) as described below.

For HE staining, tissue sections were deparaffinized and hydrated, washed in deionized water (DW), stained with hematoxylin (10 min), washed in DW, immersed in Tris-HCl buffer (pH: 7.6), washed in DW, immersed in 80% alcohol, stained with eosin (4 min), dehydrated, and finally lucidificated.

For EVG staining, tissue sections were deparaffinized and hydrated, washed in DW, incubated with resorcin-fuchsin staining solution at room temperature (RT) overnight, washed in DW, immersed in Fe-hematoxylin solution (3 min), washed with DW, immersed in Van Gieson solution (15 min), washed with 100% alcohol, dehydrated, and finally lucidificated.

For αSMA staining, endogenous peroxidase activity was blocked by treatment with 3% hydrogen peroxide (10 min). After washing in DW and immersing in Tris Buffered Saline with Tween 20 (TBST, pH 7.6; 50 mM Tris-HCl, 150 mM NaCl, and 0.05% Tween 20), sections were incubated (for 30 min) with a monoclonal antibody to α-SMA (mouse,

1A4; 1:100, M0851, Dako, Glostrup, Denmark) at RT, washed with TBST, incubated with Simple Stain Rat MAX-PO (MULTI) (714191, Nichirei Biosciences, Inc, Tokyo, Japan) at RT (30 min), washed with TBST, incubated with DAB chromogen (725191, Nichirei) (5 min), washed with DW, and finally counterstained with hematoxylin (1 min).

For CD31 staining, antigen retrieval was conducted using an antigen-retrieval solution (415211, Nichirei) at 98°C for 20 min, followed by cooling for 30 min. Then, the sections were washed in DW, treated with 3% hydrogen peroxide (10 min), washed with DW, immersed in TBST, incubated with a protein-block solution (3% BSA in PBS) at RT (60 min), incubated with an anti-CD31 antibody (rabbit, 1:10000, ab18298, Abcam, Cambridge, MA, USA) at 4°C overnight, washed with TBST, incubated with Simple Stain Rat at RT (30 min), washed with TBST, incubated with DAB chromogen (5 min), washed in DW, and finally counterstained with hematoxylin (1 min).

2.5 Statistical analysis

To analyze peptide binding, the Tukey-Kramer Honestly Significant Difference (HSD) test was performed to compare the four groups. The same HSD test was used as a *post hoc* test for a mixed model to analyze the flux value of the replanted tails. JMP Pro 14 software (SAS Institute Inc., Cary, NC, USA) was used.

3. Results

3.1 Decellularization and luminal-surface modification of rat-tail arteries

The decellularized rat-tail arteries had a mean internal diameter of 0.63 ± 0.04 mm, which was suitable for microsurgical sutures (Figure 1A) and could be handled in the same manner as the native artery. Histologically, the decellularized graft was composed of external loose connective tissue, an external elastic membrane, tunica media, and an internal elastic membrane. No cellular components were visible (Figure 1B and Supporting Information 1).

The luminal surface of the decellularized arteries was modified with CMP-REDV through heating and quenching, as described by Hwang (Figure 2).[29] The fluorescence intensities of cross sections stained with fluorescently labeled peptides were significantly high when pressurized arteries were incubated with monomeric peptide solution (Figure 3A, B). Fluorescent staining of samples pressurized at 0–1000 MPa revealed that peptide binding positively correlated with pressure during UHP treatment ($r^2 = 0.32$, $p = 0.013$) (Figure 3C, D).

3.2 *In vivo* experiments

Figure 4 shows a schematic for graft implantation in the tail replantation model. For the validation of the model, we initially confirmed that the disruption of blood flow resulted in tail necrosis. In the two control groups, three days after amputation and re-suturing, the tails with no vascular anastomosis became dark (Figure 5A), while the tails with only one arterial inflow and no venous drainage showed severe swelling with a dark-red color, suggesting venous congestion (Figure 5B). Laser speckle images of both these control groups showed no active blood flow, indicating imminent necrosis. These observations formed the premise for our analysis and discussion of the results of the tail replantation experiment on the study group.

In the study group, 12 rats underwent tail replantation. Three of the 12 replanted tails were excluded and all of the remaining nine tails survived with normal skin color for 3 weeks post-surgery. Figure 6A shows representative replanted tails. Laser-speckle contrast analysis revealed that blood flow of the amputated tails improved by a statistically significant extent by revascularization using the CMP-REDV-conjugated microvascular grafts (Figure 6B). Blood flows in replanted tails at all predetermined time points was not statistically different from those of native tails.

Ultrasound showed that all nine arterial grafts remained patent and had pulsatile blood flow at all studied time points until the final observation (Supporting Information 2). The patency rate of the venous grafts was 7/9 at 3 weeks, 4/5 at 3 months, and 3/3 at 6 months. The patency rate estimated via Kaplan-Meier test was 78%, 62%, and 62% at 3 weeks, 3 months, and 6 months, respectively (Supporting Information 3). The failed venous grafts exhibited wall collapse, but thrombosis was not detected (data not shown). Even in cases in which the reconstructed vein was occluded, the laser-speckle flux of the replanted tails was not statistically different from that of native tails (Figure 6C).

After 6 months, the arterial grafts appeared to have regenerated into neoarteries with opaque, thick vascular walls (Figure 7A). Figure 8 shows the remodeling and regeneration of the arterial grafts. Cells expressing CD31 were present on the luminal surface and round cell infiltration was observed at 3 weeks. At 3 months, a thick neo-tunica media containing cells expressing αSMA was observed inside the original tunica media. Three months later, i.e. 6 months post-surgery, αSMA was upregulated and vascular smooth muscle cells (VSMCs) were clearly observed in the neo-tunica media (thickness: 95.0 ± 28.0 μm) (Figure 8B). In contrast with the arterial grafts, the venous grafts regenerated into neoveins, with a thin vascular wall. Gross explant analysis at 6 months revealed a smooth and thin inner surface (Figure 7B). Figure 9

shows a representative model of venous grafts. At 3 weeks, cells expressing CD31 aligned on the luminal surface of the venous graft. The original tunica media degraded within 3–6 months, and a thin neo-tunica media (thickness: 9.3 ± 1.7 μm) wall containing cells expressing αSMA regenerated between the original internal elastic membrane and neointima.

4. Discussion

Tail replantation using CMP-REDV conjugated microvascular grafts was successful in all cases, in contrast with the control devascularization and venous-congestion models, which exhibited total necrosis. The arterial grafts showed a 100% patency rate, whereas two of the nine venous grafts were occluded by 3 weeks. Because of the low-flow and low-pressure venous circulation, blood flow in the venous grafts was probably interrupted via postoperative edema, hematoma, and active motion of the tail. Nevertheless, the most important point is that tails with failed venous grafts displayed no evidence of venous congestion. The implants remained patent at least until the collateral vein had been regenerated and the venous drainage through the venous grafts in the early stage was sufficient for the survival of small-tissue tails.[32]

To develop decellularized tissue-based small-diameter vascular prostheses, researchers have investigated multiple methods to improve thrombogenic potential.[12,14,33-37] One method is pre-seeding of autologous endothelial cells, but it is unsuitable for generating off-the-shelf products.[14] Vascular endothelial growth factors and brain-derived neurotrophic factors have been immobilized on decellularized graft lumens,[36,37] but whether they function in long-length grafts, or how they affect long-term remodeling of materials, have not been satisfactorily elucidated. Other modifications for decellularized blood vessels, such as heparin immobilization[14,38] and increased vascular wall porosity using laser perforations,[39] have not been shown to be effective for submillimeter-diameter vessels. On the other hand, the efficacy of CMP-REDV has already been confirmed with two long-length decellularized vessels with different IDs: the ostrich-carotid artery (ID 2–4 mm, length 30 cm) and the rat-tail artery (ID 0.6 mm, length 5 cm), with the advantage of long length, uniform ID and fewer branches.[7,25] CMP-REDVs are known to induce antithrombotic interfaces and promote neointima formation in very long grafts, where migration of vascular cells from native vessels are not expected. Although this study was limited to short grafts, the presence of CD31-positive cells at the central position of the graft at 3 weeks post-implantation may be a product of the cell-capturing effect of CMP-REDVs, because endothelial-cell

migration from the native arteries to the grafts without CMP-REDVs was observed only up to 1 mm from the suture line at 3 weeks in a previous study (Supporting Information 4).[7] Moreover, this study demonstrates that CMP-REDV-conjugated grafts show positive remodeling at 6 months. Interestingly, the grafts have been reported to remodel differently depending on whether they are implanted into an artery or a vein, thereby suggesting that biomechanical signaling, such as pressure and fluid shear stress, is a major driving force in the maturation of vascular wall bioscaffolds.[40-43] In addition, although preliminary, a neoartery extracted at 6 months displayed sensitivity to vasodilators and vasoconstrictors (n = 1, Supporting Information 5). To date, only a few studies have reported vasomotor function of neoarteries regenerated from acellular vascular grafts.[40,44-46]

The UHP treatment facilitates effective elimination of cellular components without detergents,[47,48] suppresses viral activity,[49] and influences subsequent luminal-surface modification. In addition, UHP treatment slightly denatures native-tissue collagen, increasing its CMP-binding sites. Since CMPs cannot interact with intact collagen,[27-29] UHP treatment is indispensable for CMP binding as well as decellularization. In our previous study, 2 mm ID decellularized vessels were heated to 60 °C within the peptide solution to immobilize CMP-REDVs. However, in cases of submillimeter-diameter

vessels with very thin and fragile vessel walls, thermal denaturation of the extracellular matrices resulted in poor patency associated with decreased graft compliance, although it did increase peptide-binding sites. Hwang described the method for monomerizing peptides by a heating and quenching protocol to immobilize CMPs without thermal denaturation of target tissues,[29] which may be suitable for immobilizing CMP-REDVs to very small-diameter decellularized vessels.

This study has some limitations. First, this study lacked sample size calculation, animal blinding, a non REDV-modified graft control group, and any form of quantitative analysis. Second, thrombogenic mechanisms in rats are different from those in humans.[50] Future studies should be focused on implanting longer arterial/venous grafts in large-animal models and analyzing vasomotor function of neovessels with an adequate sample size. Finally, decellularized tissues should be evaluated for their biological safety in accordance with ISO10993 (Biological evaluation of medical devices).

5. Conclusion

This study describes the potential utility of allogenic CMP-REDV-conjugated

microvascular grafts for small-tissue replantation. All rat tails survived by arterial and venous reconstruction using microvascular grafts. The 6-month patency rate was 100% in arterial grafts and 62% in venous grafts. Two venous grafts were occluded by 3 weeks but displayed no sign of tail-venous congestion, suggesting that the implants remained patent at least until the collateral vein was regenerated. Furthermore, arterial and venous grafts remodeled differently to regenerate into corresponding neovessels. However, further investigations using larger animal models are required for better understanding of the process and for determining the actual scope of its potential application in humans.

References

1. Classen DA. The indications and reliability of vein graft use in free flap transfer. Can J Plast Surg 2004;12:27-29.
2. Nelson JA, Fischer JP, Grover R, et al. Vein grafting your way out of trouble: Examining the utility and efficacy of vein grafts in microsurgery. J Plast Reconstr Aesthet Surg 2015;68:830-836.
3. Bayramicli M, Tetik C, Sonmez A, Gurunluoglu R, Baltaci F. Reliability of primary vein grafts in lower extremity free tissue transfers. Ann Plast Surg 2002;48:21-29.

4. Sakamoto S, Hattori Y, Doi K, Moriya A. The efficacy of interpositional vein grafts in fingertip replantation [in Japanese]. J Jpn Soc Surg Hand 2009;25:738–740.

5. Alpert BS, Buncke HJ, Brownstein M. Replacement of damaged arteries and veins with vein grafts when replanting crushed, amputated fingers. Plast Reconstr Surg 1978;61:17-22.

6. Sebastin SJ, Chung KC. A systematic review of the outcomes of replantation of distal digital amputation. Plast Reconstr Surg 2011;128:723-737.

7. Yamanaka H, Yamaoka T, Mahara A, Morimoto N, Suzuki S. Tissue-engineered submillimeter-diameter vascular grafts for free flap survival in rat model. Biomaterials 2018;179:156-163.

8. Shen TY, Mitchell GM, Morrison WA, O'Brien BM. The use of long synthetic microvascular grafts to vascularise free flaps in rabbits. Br J Plast Surg 1988;41:305-312.

9. Weinberg CB, Bell E. A blood vessel model constructed from collagen and cultured vascular cells. Science 1986;231:397-400.

10. Radke D, Jia W, Sharma D, et al. Tissue Engineering at the Blood-Contacting Surface: A Review of Challenges and Strategies in Vascular Graft Development. Adv Healthc Mater 2018;7:e1701461.

11. Pashneh-Tala S, MacNeil S, Claeyssens F. The Tissue-Engineered Vascular Graft-Past, Present, and Future. Tissue Eng Part B-Re 2016;22:68-100.

12. Zou T, Fan J, Fartash A, Liu H, Fan Y. Cell-based strategies for vascular regeneration. J Biomed Mater Res A 2016;104:1297-1314.

13. Row S, Santandreu A, Swartz DD, Andreadis ST. Cell-free vascular grafts: Recent developments and clinical potential. Technology (Singap World Sci) 2017;5:13-20.

14. Ilanlou S, Khakbiz M, Amoabediny G, Mohammadi J. Preclinical studies of acellular extracellular matrices as small-caliber vascular grafts. Tissue Cell 2019;60:25-32.

15. Crapo PM, Gilbert TW, Badylak SF. An overview of tissue and whole organ decellularization processes. Biomaterials 2011;32:3233-3243.

16. Goins A, Webb AR, Allen JB. Multi-layer approaches to scaffold-based small diameter vessel engineering: A review. Mater Sci Eng C Mater Biol Appl 2019;97:896-912.

17. Seifu DG, Purnama A, Mequanint K, Mantovani D. Small-diameter vascular tissue engineering. Nat Rev Cardiol 2013;10:410-421.

18. Cleary MA, Geiger E, Grady C, Best C, Naito Y, Breuer C. Vascular tissue engineering: the next generation. Trends Mol Med 2012;18:394-404.

19. Munisso MC, Yamaoka T. Circulating endothelial progenitor cells in small-diameter artificial blood vessel. J Artif Organs 2019.

20. Mahara A, Sakuma T, Mihashi N, Moritan T, Yamaoka T. Accelerated endothelialization and suppressed thrombus formation of acellular vascular grafts by modifying with neointima-inducing peptide: A time-dependent analysis of graft patency in rat-abdominal transplantation model. Colloids Surf B Biointerfaces 2019;181:806-813.

21. Liu Y, Munisso MC, Mahara A, et al. A surface graft polymerization process on chemically stable medical ePTFE for suppressing platelet adhesion and activation. Biomater Sci 2018;6:1908-1915.

22. Klemm D, Schumann D, Udhardt U, Marsch S. Bacterial synthesized cellulose — artificial blood vessels for microsurgery. Prog Polym Sci 2001;26:1561–1603.

23. Andrade FK, Silva JP, Carvalho M, Castanheira EM, Soares R, Gama M. Studies on the hemocompatibility of bacterial cellulose. J Biomed Mater Res A 2011;98:554-566.

24. Li X, Xu J, Nicolescu CT, Marinelli JT, Tien J. Generation, Endothelialization, and Microsurgical Suture Anastomosis of Strong 1-mm-Diameter Collagen Tubes. Tissue Eng Part A 2017;23:335-344.

25. Mahara A, Somekawa S, Kobayashi N, et al. Tissue-engineered acellular small diameter long-bypass grafts with neointima-inducing activity. Biomaterials 2015;58:54-62.

26. Hubbell JA, Massia SP, Desai NP, Drumheller PD. Endothelial cell-selective materials for tissue engineering in the vascular graft via a new receptor. Biotechnology (N Y) 1991;9:568-572.

27. Wang AY, Mo X, Chen CS, Yu SM. Facile modification of collagen directed by collagen mimetic peptides. J Am Chem Soc 2005;127:4130-4131.

28. Mo X, An YJ, Yun CS, Yu SM. Nanoparticle-assisted visualization of binding interactions between collagen mimetic peptide and collagen fibers. Angew Chem Int Edit 2006;45:2267-2270.

29. Hwang J, Huang Y, Burwell TJ, et al. In Situ Imaging of Tissue Remodeling with Collagen Hybridizing Peptides. ACS Nano 2017;11:9825-9835.

30. Gill TJ, 3rd, Kunz HW, Misra DN, Hassett AL. The major histocompatibility complex of the rat. Transplantation 1987;43:773-785.

31. Acland R. Signs of patency in small vessel anastomosis. Surgery 1972;72:744-748.

32. Black MJ, Chait L, O'Brien BM, Sykes PJ, Sharzer LA. How soon may the axial

vessels of a surviving free flap be safely ligated: a study in pigs. Br J Plast Surg 1978;31:295-299.

33. Zhou M, Liu Z, Li K, et al. Beneficial effects of granulocyte-colony stimulating factor on small-diameter heparin immobilized decellularized vascular graft. J Biomed Mater Res A 2010;95:600-610.

34. Kang J, Lee BW, Kim JH, et al. Granulocyte colony-stimulating factor minimizes negative remodeling of decellularized small diameter vascular graft conduits but not medial degeneration. Ann Vasc Surg 2013;27:487-496.

35. Koobatian MT, Row S, Smith RJ, Jr., Koenigsknecht C, Andreadis ST, Swartz DD. Successful endothelialization and remodeling of a cell-free small-diameter arterial graft in a large animal model. Biomaterials 2016;76:344-358.

36. Iijima M, Aubin H, Steinbrink M, et al. Bioactive coating of decellularized vascular grafts with a temperature-sensitive VEGF-conjugated hydrogel accelerates autologous endothelialization in vivo. J Tissue Eng Regen Med 2018;12:e513-e522.

37. Zeng W, Wen C, Wu Y, et al. The use of BDNF to enhance the patency rate of small-diameter tissue-engineered blood vessels through stem cell homing mechanisms. Biomaterials 2012;33:473-484.

38. Conklin BS, Richter ER, Kreutziger KL, Zhong DS, Chen C. Development and evaluation of a novel decellularized vascular xenograft. Med Eng Phys 2002;24:173-183.

39. Bergmeister H, Boeck P, Kasimir MT, et al. Effect of laser perforation on the remodeling of acellular matrix grafts. J Biomed Mater Res B Appl Biomater 2005;74:495-503.

40. Zhu M, Wu Y, Li W, et al. Biodegradable and elastomeric vascular grafts enable vascular remodeling. Biomaterials 2018;183:306-318.

41. Roh JD, Nelson GN, Brennan MP, et al. Small-diameter biodegradable scaffolds for functional vascular tissue engineering in the mouse model. Biomaterials 2008;29:1454-1463.

42. Qiu J, Zheng Y, Hu J, et al. Biomechanical regulation of vascular smooth muscle cell functions: from in vitro to in vivo understanding. J R Soc Interface 2014;11:20130852.

43. Zhang XQ, Bendeck MP, Simmons CA, Santerre JP. Deriving vascular smooth muscle cells from mesenchymal stromal cells: Evolving differentiation strategies and current understanding of their mechanisms. Biomaterials 2017;145:9-22.

44. Allen RA, Wu W, Yao M, et al. Nerve regeneration and elastin formation within

poly(glycerol sebacate)-based synthetic arterial grafts one-year post-implantation in a rat model. Biomaterials 2014;35:165-173.

45. Sakakibara S, Ishida Y, Hashikawa K, Yamaoka T, Terashi H. Intima/medulla reconstruction and vascular contraction-relaxation recovery for acellular small diameter vessels prepared by hyperosmotic electrolyte solution treatment. J Artif Organs 2014;17:169-177.

46. Huynh T, Abraham G, Murray J, Brockbank K, Hagen PO, Sullivan S. Remodeling of an acellular collagen graft into a physiologically responsive neovessel. Nat Biotechnol 1999;17:1083-1086.

47. Fujisato T, Minatoya K, Yamazaki S, et al. Cardiovascular regeneration therapies using tissue engineering approaches. Springer, Tokyo 2005:83-94.

48. Funamoto S, Nam K, Kimura T, et al. The use of high-hydrostatic pressure treatment to decellularize blood vessels. Biomaterials 2010;31:3590-3595.

49. Lou F, Neetoo H, Chen H, Li J. High hydrostatic pressure processing: a promising nonthermal technology to inactivate viruses in high-risk foods. Annu Rev Food Sci Technol 2015;6:389-409.

50. Swartz DD, Andreadis ST. Animal models for vascular tissue-engineering. Curr Opin Biotechnol 2013;24:916-925.

Figure Legends

Figure 1. Decellularized rat tail artery. (**A**) Gross appearance of a decellularized graft; scale bars, 10 mm (*left*) and 1 mm (*right*). (**B**) Histological staining of the decellularized graft comprising external loose connective tissue, external elastic membrane (white arrowheads), tunica media, and internal elastic membrane (black arrowheads); scale bar, 50 μm. (*above, left*) HE staining. (*above, right*) EVG staining. (*below, left*) αSMA staining. (*below, right*) CD31 immunostaining.

Figure 2. Schematic of peptide modification.[29] Monomeric peptides interact with denatured collagen via strand invasion.

Figure 3. Peptide binding to pressurized tissues. (**A**) (*left*) Confocal micrographs of representative cross sections of native and 1000-MPa pressurized arteries, stained with trimeric- or monomeric Alexa Fluor 633-labeled CMP-REDVs; scale bar, 200 μm. (*right*) Comparison of peptide binding; mean gray values were estimated using ImageJ software. Monomeric peptides can interact with only the pressurized artery (n = 6, mean ± SD); *, $p < 0.01$; ***, $p < 0.0001$. (**B**) (*left*) Confocal micrographs of representative cross

sections of UHP-treated arteries (0, 50, 100, 200, 500, and 1000 Mpa) stained with monomeric Alexa Fluor 633-labeled CMP-REDVs (n = 3); scale bar, 200 μm. (*right*) Association between pressure and peptide binding (mean ± SD). Peptide binding positively correlated with pressure during UHP treatment (r^2 = 0.32, p = 0.013).

Figure 4. Schematic of rat-tail replantation; 8-mm grafts were implanted to reconstruct arterial inflow (black arrowheads) and 5-mm grafts were implanted to reconstruct venous outflow (white arrowheads).

Figure 5. Control groups. (**A**) Rat-tail devascularization model (n = 3). (*left*) Representative case from the devascularization group. (*1*) The rat tail was completely amputated and then sutured back onto the original location without vessel reconstruction. (*2*) Immediately after skin closure (0 d). The tail skin exhibited a white color, suggesting complete devascularization. (*3*) Three days after devascularization (3 d). The tail had a darker color and appeared to be inviable. (*4–6*) Laser-speckle images of devascularized tails: native tail (*4*), 0 d (*5*), and 3 d (*6*). (*right*) Median flux value over time (mean ± SD). (**B**) Rat-tail venous congestion model (n = 3). (*left*) Representative case from the venous congestion group. (1) The rat tail was completely amputated except for the tail artery and

then sutured back onto the original location without venous reconstruction. (2) Immediately after skin closure (0 d). The tail skin had an almost normal color; however, capillary refill was brisk. (3) Three days after blocking venous out-flow (3 d). The tail showed severe swelling with a dark-red color and appeared to be inviable. (4–6) Laser-speckle images of venous-congestive tails: native tail (4), 0 d (5), and 3 d (6). (*right*) Median flux value at each time point (mean ± SD).

Figure 6. (**A**) Representative case of replantation. (*above*) The rat tail was amputated at a position 1.5-cm distal to its base. (*center*) Immediately after replantation. (*below*) After 3 weeks, the replanted tail had normal skin color, in contrast to the pale, amputated tail. (**B**) Blood flow of native tail (n = 12), amputated (n = 12), and replanted tails at postoperative 3 weeks (3W, n = 9), 3 months (3M, n = 6), and 6 months (6M, n = 3). (*above*) Median flux value at each time point measured with laser-speckle contrast imaging (mean ± SD); *, $p < 0.01$; ***, $p < 0.0001$. Blood flow of the amputated tail was re-established by graft implantation and was maintained for 6 months. (*below*) Representative laser-speckle images at each time point. (**C**) Comparative assessment of median flux value measured with laser-speckle contrast imaging between cases with patent venous grafts (n = 9) and cases with venous grafts occluded by 3W (n =2).

Venous graft occlusion after autonomization of the replanted tails did not affect their blood flow (mean ± SD).

Figure 7. Luminal surface of explants at 6 months; scale bar, 5 mm. Arrows indicate suture lines. (*left*) Graft implanted into the tail artery. (*right*) Graft implanted into the tail vein.

Figure 8. Remodeling of grafts implanted into the tail artery. (**A**) Histology of the native artery and explants; 3W, 3 weeks; 3M, 3 months; 6M, 6 months; scale bar, 50 μm. The original internal elastic membrane was clearly EVG-stained (arrowheads). (**B**) (*left*) Magnified view of HE staining at 6M, showing the neo-tunica media (*1*) and the original tunica media (*2*); arrowheads, the original internal elastic membrane; scale bar, 50 μm. (*right*) Regenerated VSMCs (arrows) were circumferentially observed in the neo-tunica media; scale bar, 10 μm.

Figure 9. Remodeling of grafts implanted into the tail vein. (**A**) Histology of the native vein and explants; 3W, 3 weeks; 3M, 3 months; 6M, 6 months; scale bar, 50 μm. (**B**) Magnified view of HE staining at 6M; scale bar, 50 μm. Over 3–6 months, the original

tunica media (*2*) was almost degraded, and a thin neo-tunica media (*1*) with cells expressing αSMA formed on the original internal elastic membrane (arrowheads).

(A)

(B)

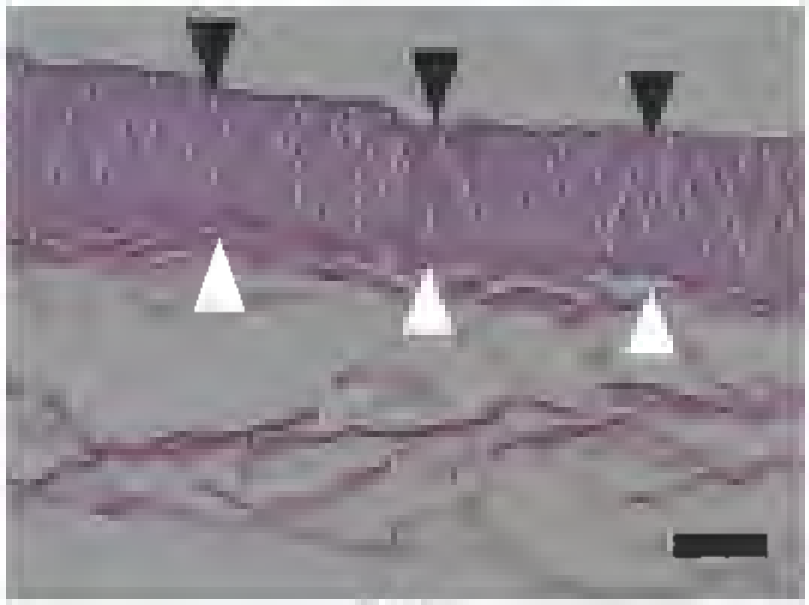

HE

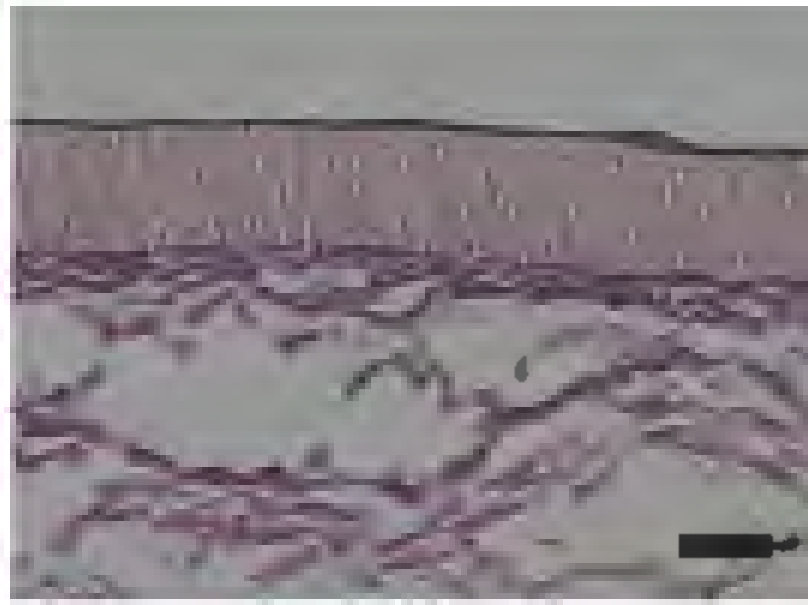

EVG

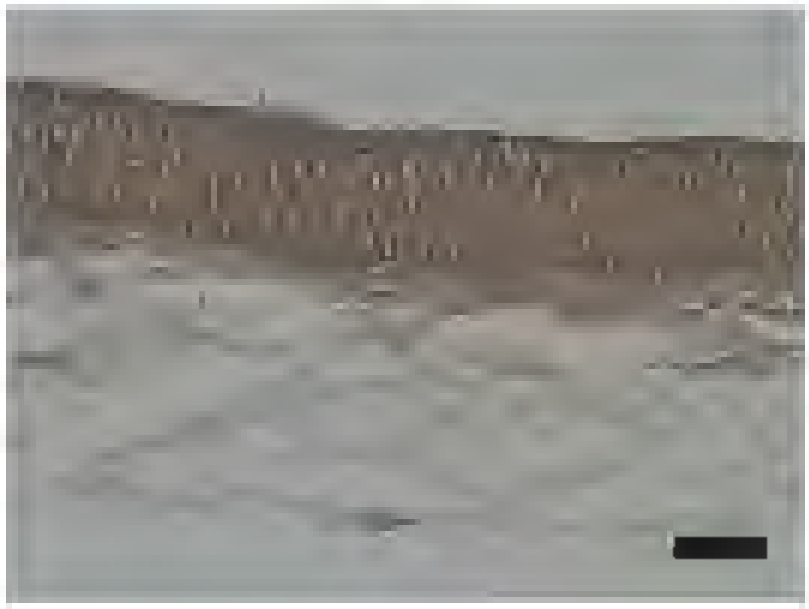

αSMA

CD31

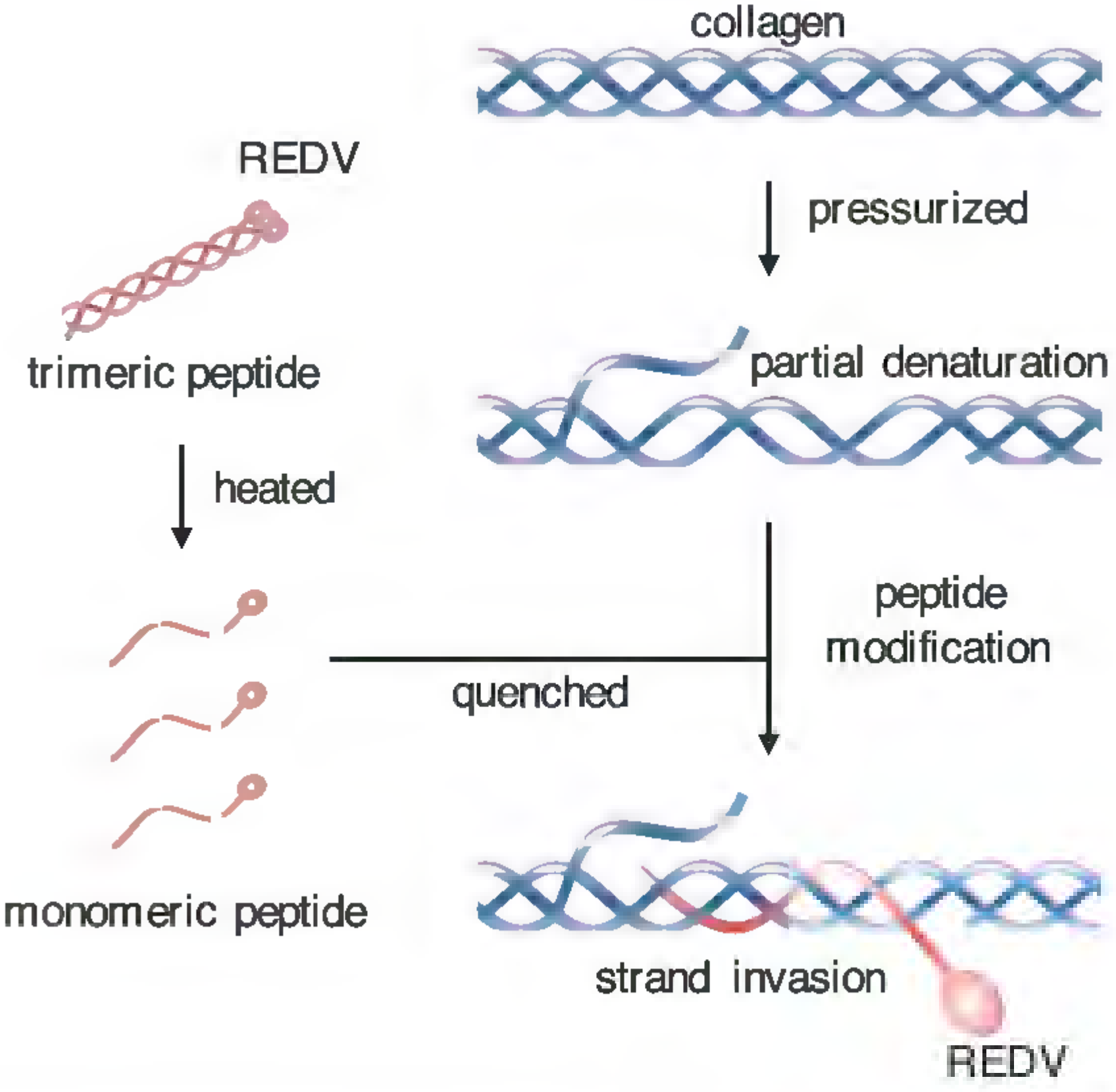
collagen
REDV
pressurized
trimeric peptide
partial denaturation
heated
peptide
modification
quenched
monomeric peptide
strand invasion
REDV

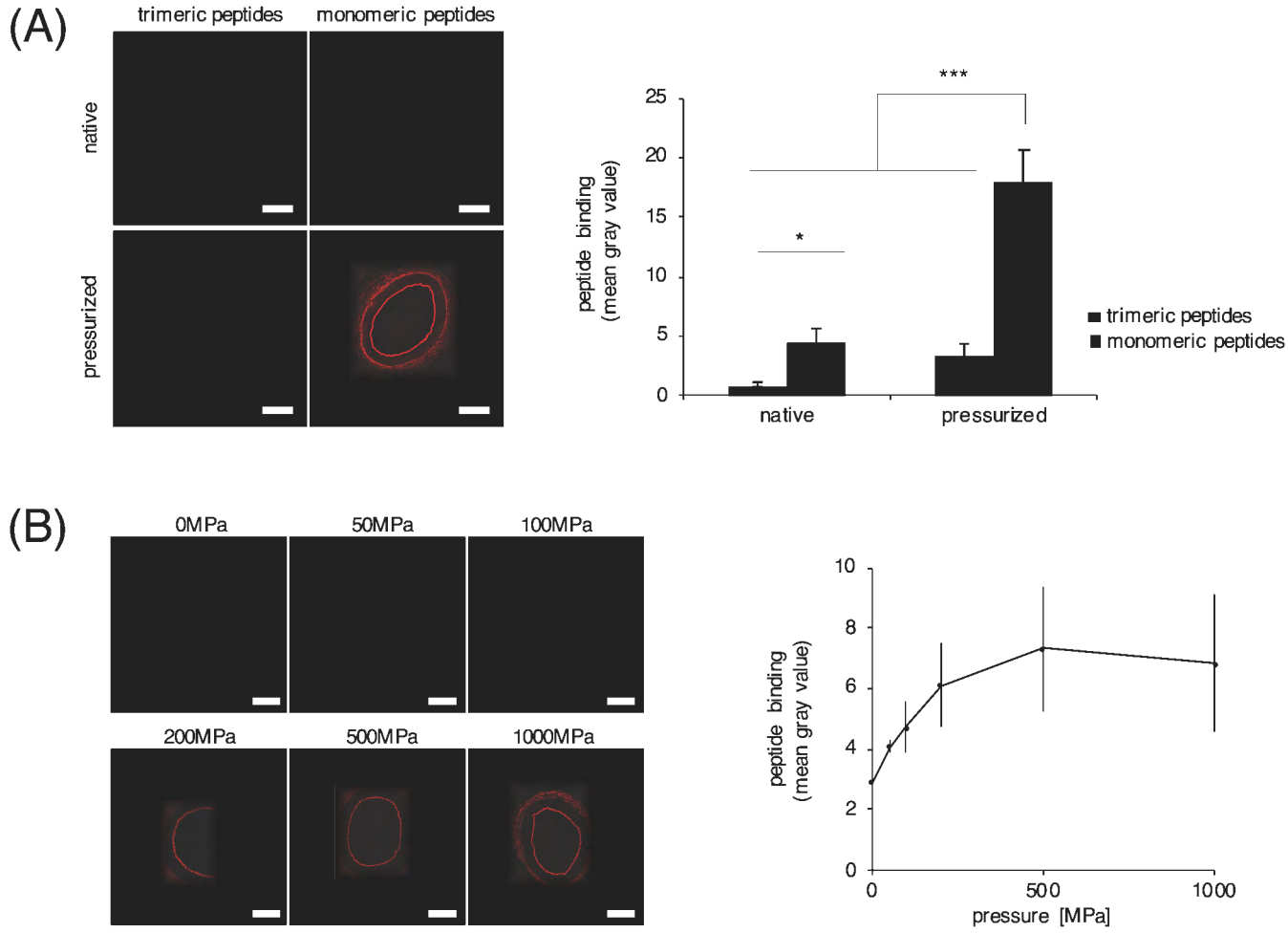
(A)
trimeric peptides
monomeric peptides
native
pressurized
peptide binding
(mean gray value)
25
20
15
10
5
0
***
*
native
pressurized
trimeric peptides
monomeric peptides
(B)
0MPa
50MPa
100MPa
200MPa
500MPa
1000MPa
peptide binding
(mean gray value)
10
8
6
4
2
0
0
500
1000
pressure [MPa]

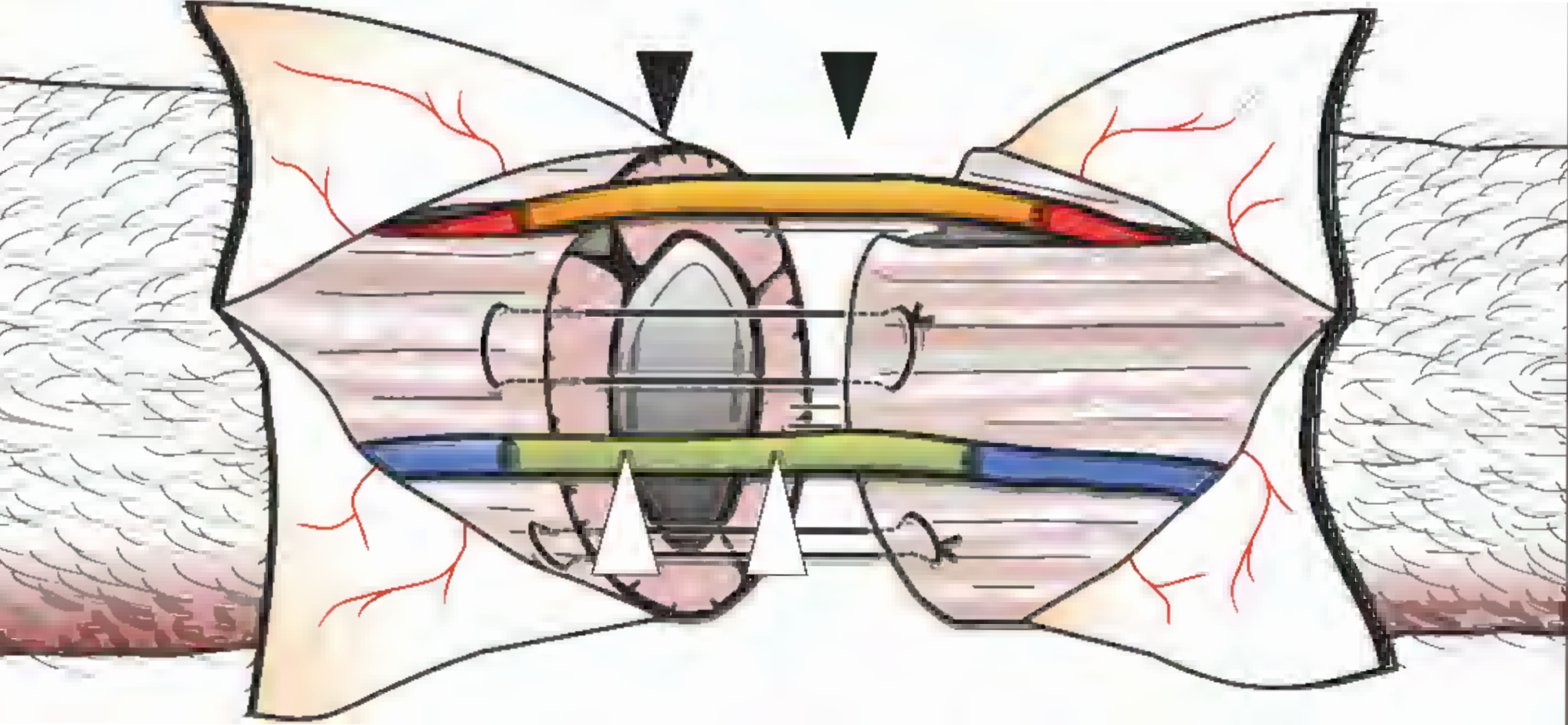

(A)

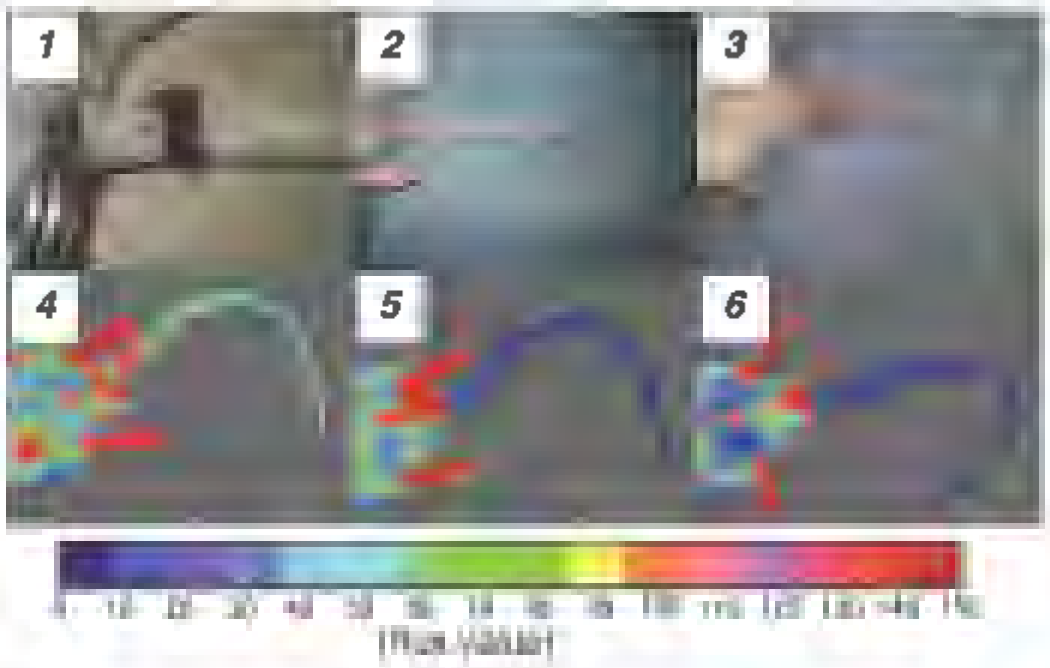
1
2
3
4
5
6

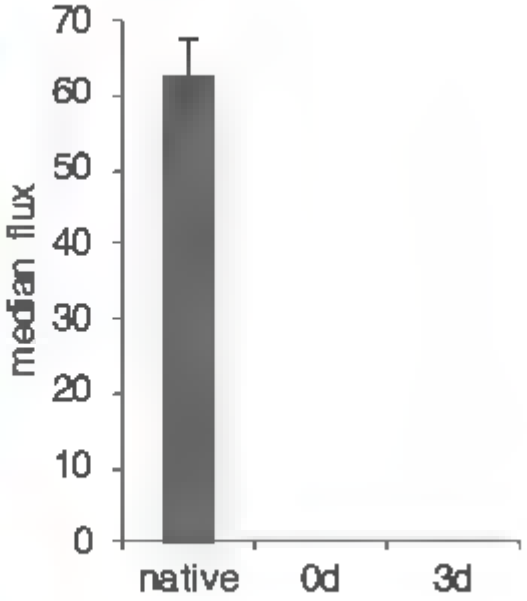
70
60
50
40
30
20
10
0
median flux
native
0d
3d

(B)

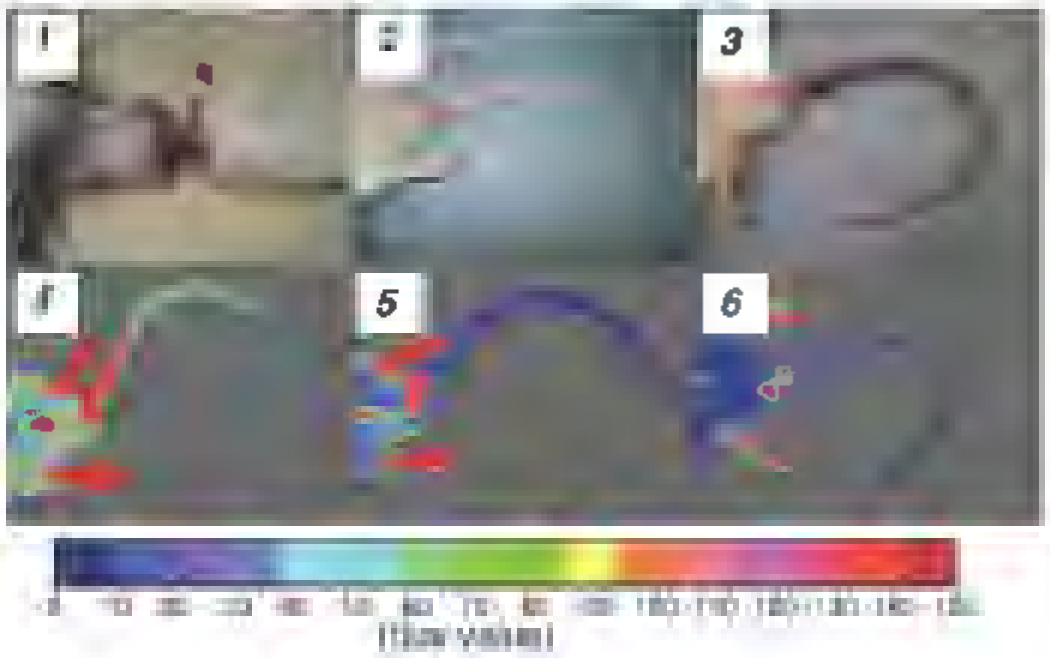
3
5
6

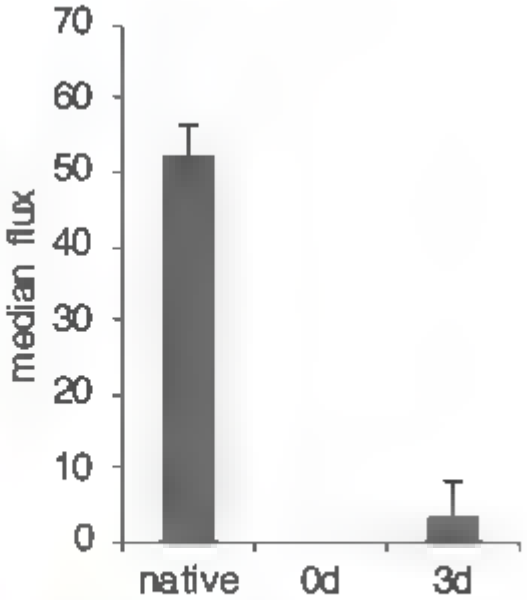
70
60
50
40
30
20
10
0
median flux
native
0d
3d

(A)

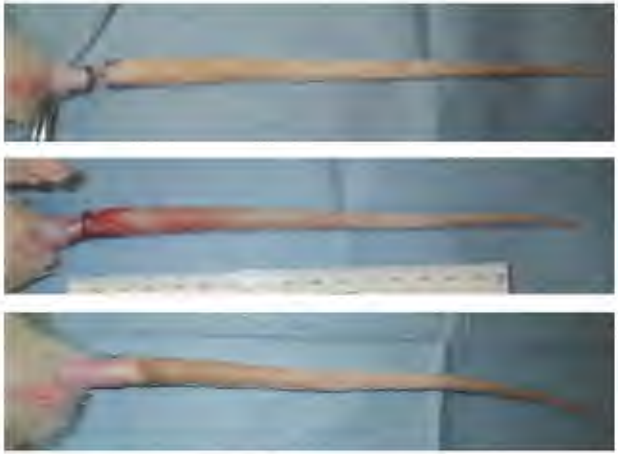

(B)

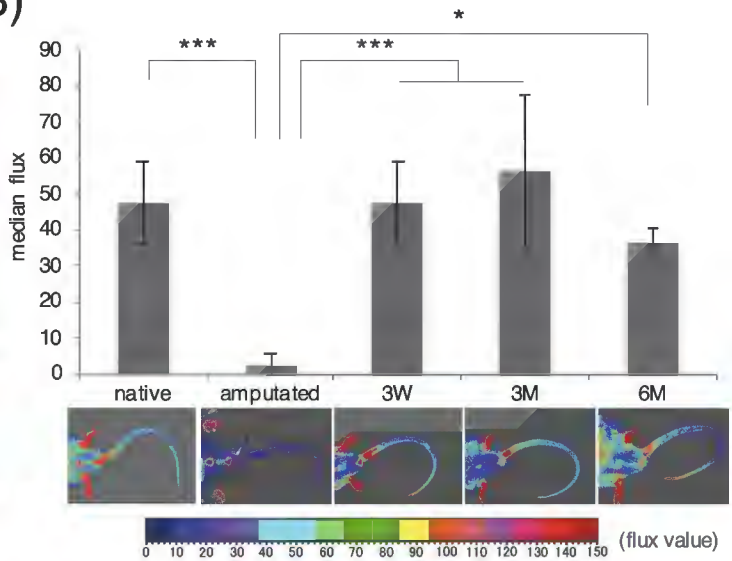
***
***
*
median flux
90
80
70
60
50
40
30
20
10
0
native
amputated
3W
3M
6M
0 10 20 30 40 50 60 70 80 90 100 110 120 130 140 150
(flux value)

(C)

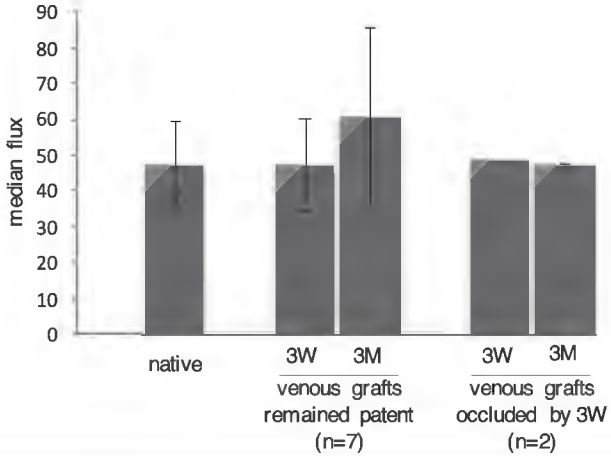
median flux
90
80
70
60
50
40
30
20
10
0
native
3W
3M
venous grafts remained patent (n=7)
3W
3M
venous grafts occluded by 3W (n=2)

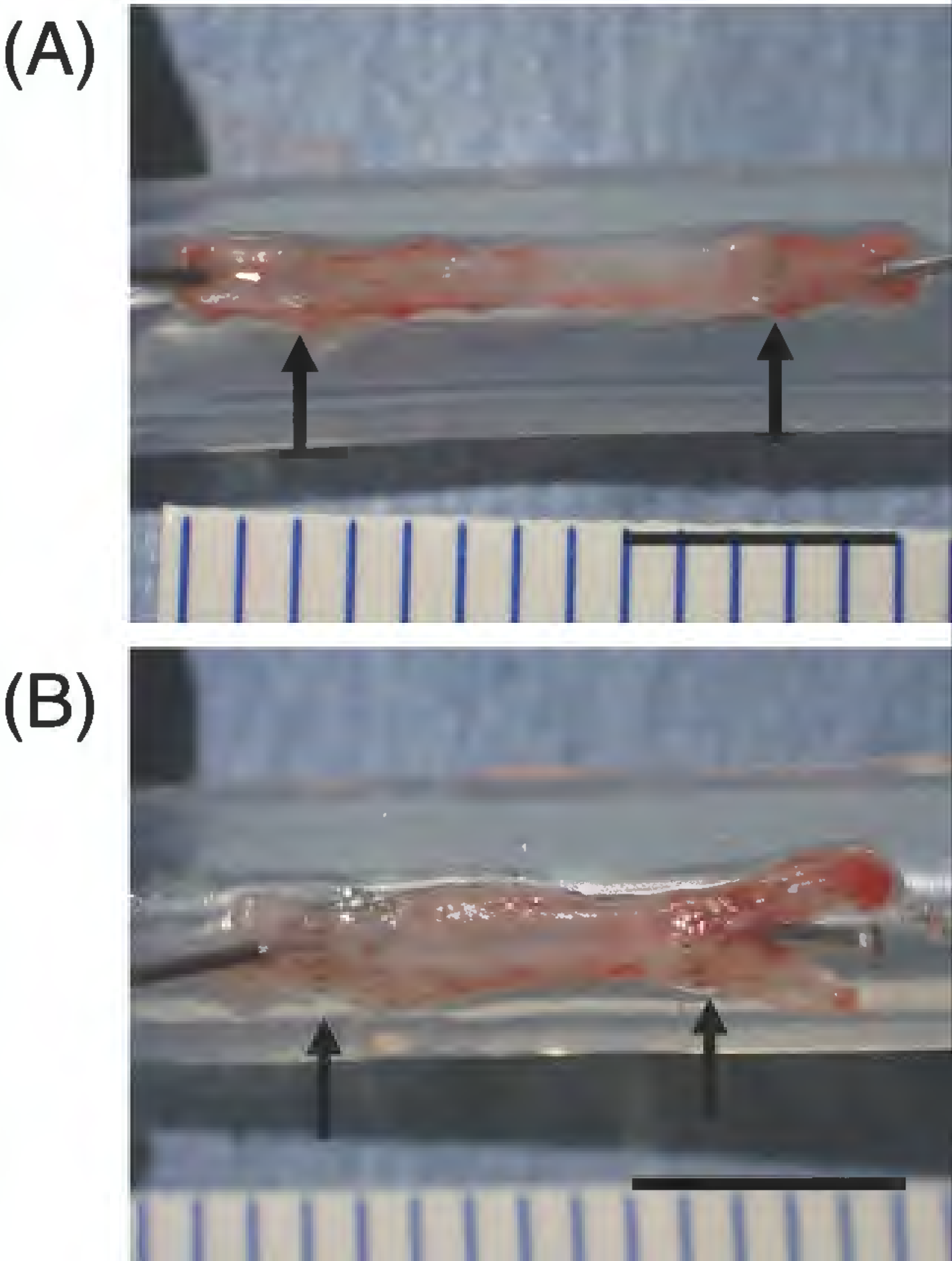
(A)
(B)

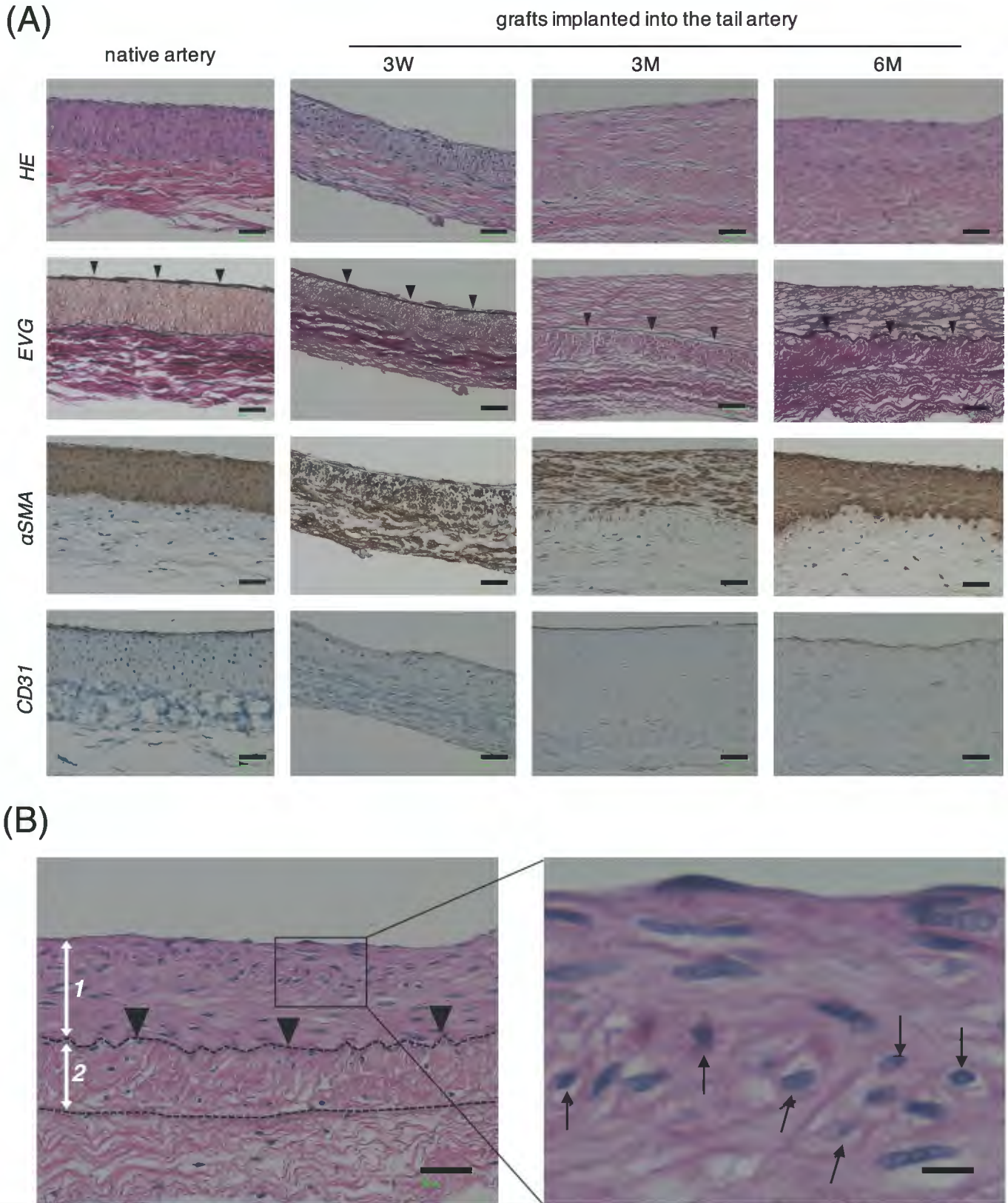
(A)
grafts implanted into the tail artery
native artery
3W
3M
6M
HE
EVG
αSMA
CD31
(B)
1
2

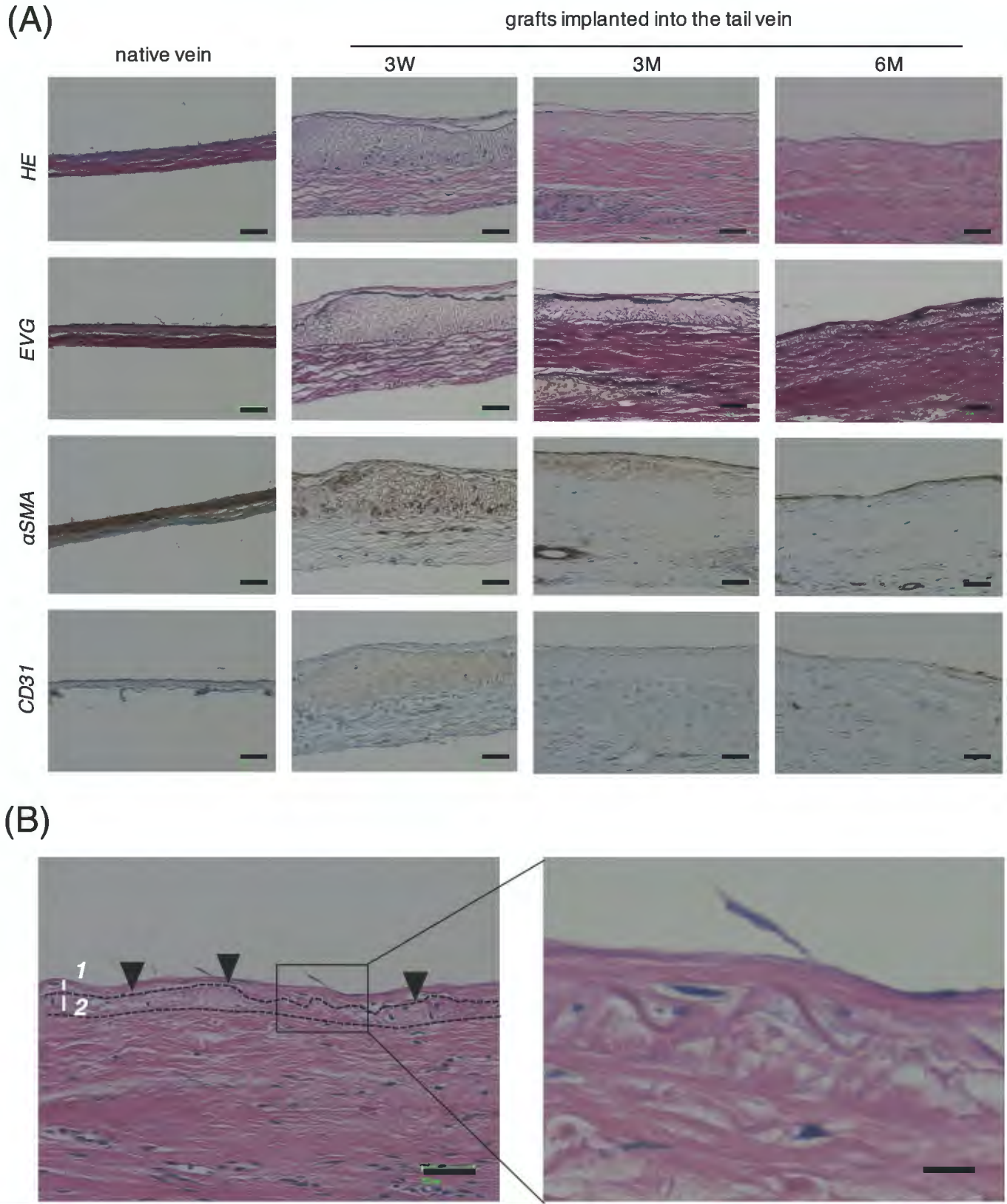
(A)
grafts implanted into the tail vein
native vein
3W
3M
6M
HE
EVG
αSMA
CD31
(B)
1
2

Supporting Information 1

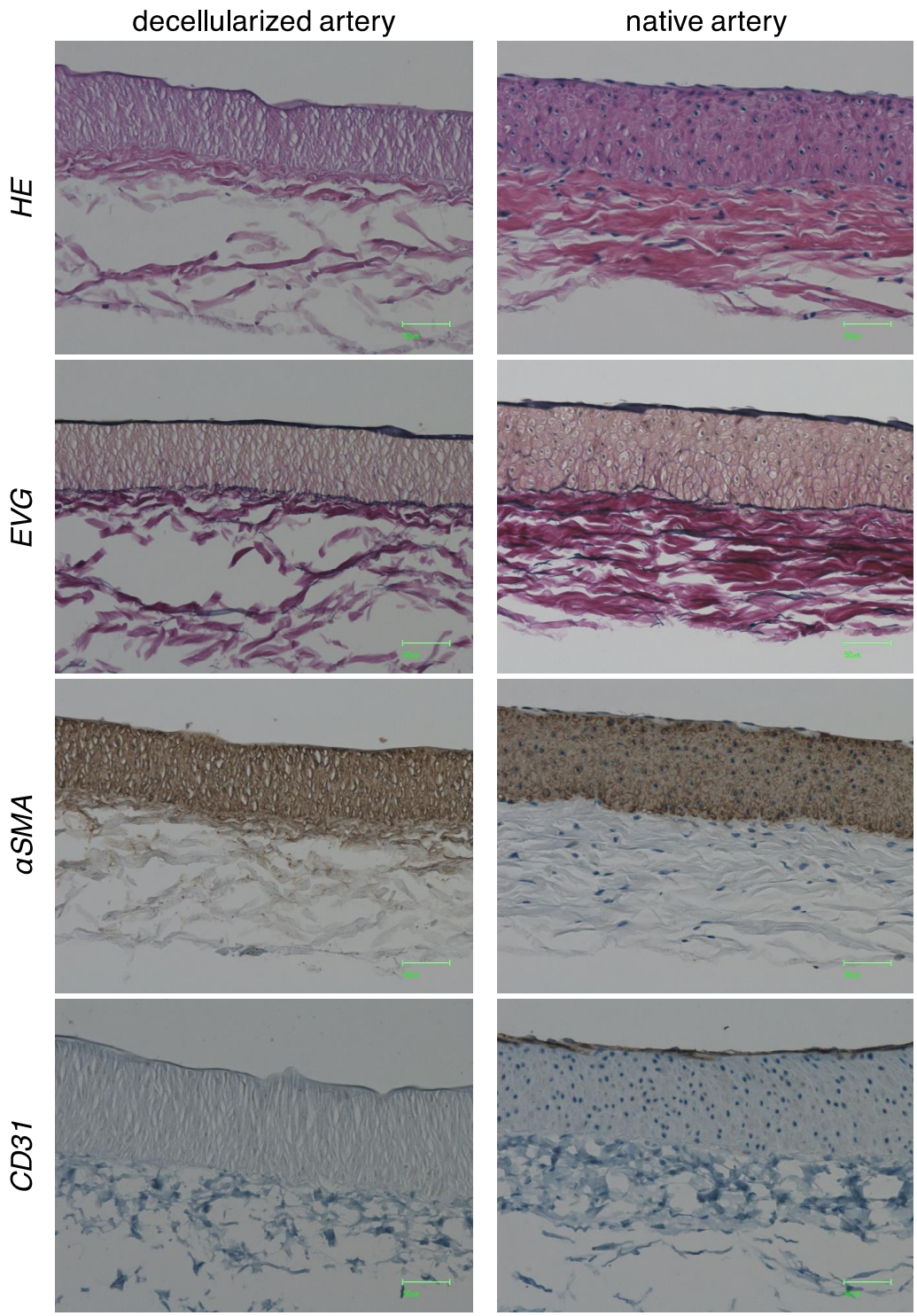

Figure. Histological images of decellularized artery and native artery.

Supporting Information 2

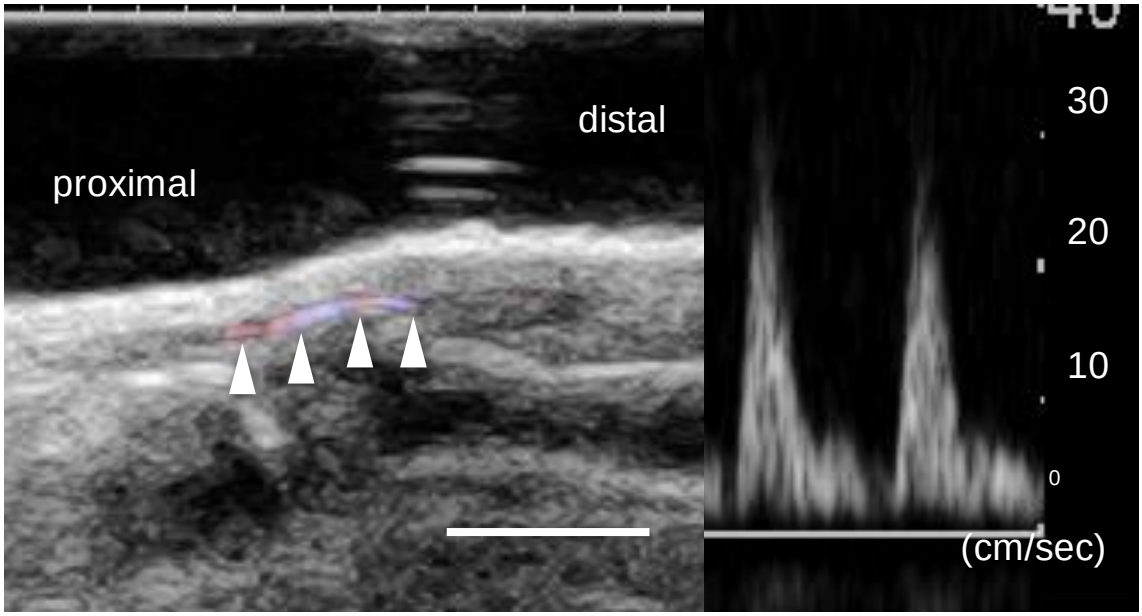

Figure. Laser Doppler ultrasound imaging of graft patency and pulsatile blood flow at postoperative 6 months; scale bar, 5 mm. Arrowheads indicate the neoartery.

Supporting Information 3

Table. Summary of patency; P, patent; 0cl, occluded.

rat	follow up	artery			vein		
		3W	3M	6M	3W	3M	6M
#1	3W	P			P		
#2		P			Ocl		
#3		P			P		
#4	3M	P	P		P	P	
#5		P	P		Ocl	Ocl	
#6		P	P		P	Ocl	
#7	6M	P	P	P	P	P	P
#8		P	P	P	P	P	P
#9		P	P	P	P	P	P

Supporting Information 4

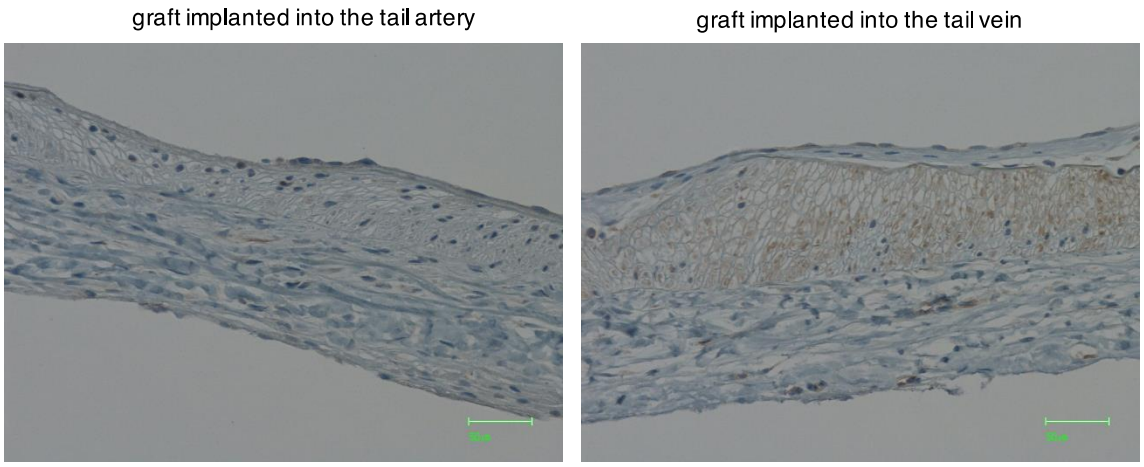

Figure. Histological images of CD31 staining at 3W.
Cells expressing CD31 were located on luminal surfaces of both grafts.

Supporting Information 5

Evaluation of neoartery vasomotor function

Methods

Vasomotor function of one arterial graft extracted at 6M (neoartery) was preliminary evaluated. Each sample, including the neoartery, native artery, and decellularized graft before implantation, was connected in a closed circuit filled with saline and incubated in a constant temperature bath containing saline at 37 ° C. The internal pressure of the circuit was maintained at 100 mmHg. Noradrenaline was supplemented at a final concentration of 10 μM to the constant-temperature bath; 3 min later, papaverine hydrochloride was added to a final concentration of 0.6 mM. The outer diameter was monitored with a CCD camera (C2400; Hamamatsu Photonics, Co., Ltd., Hamamatsu, Japan) during the administration of vaso-drugs, and relative changes in the outer diameter were compared in each sample.

Results

The decellularized graft before implantation had no vasomotor function. Both the neoartery and the native artery contracted in response to noradrenaline (diameter change: 7.5% in the neoartery and 22.2% in the native artery) and relaxed in response to papaverine.

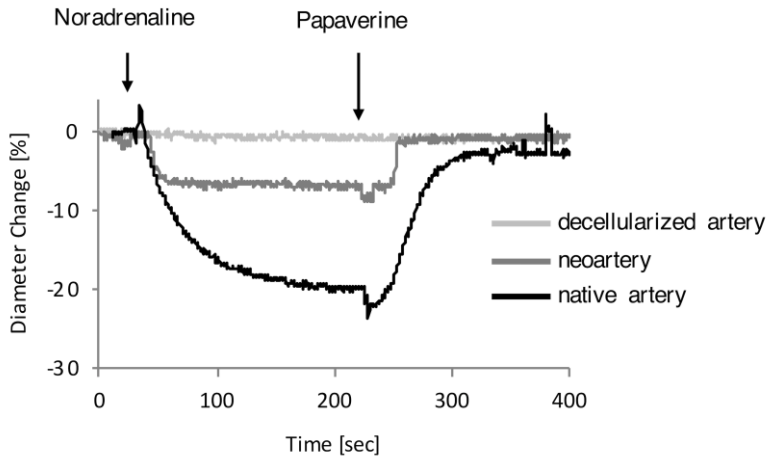

Figure. Evaluation of vasomotor function.
Relative change in outer diameter was measured during administration of vaso-drugs (arrows).